Matrix Biology 145 (2026) 75–88

Contents lists available at ScienceDirect

Matrix Biology

journal homepage: www.elsevier.com/locate/matbio

Arylsulfatase I is a novel lysosomal chondroitin endosulfatase regulating endochondral ossification

Rafaela Grecco-Machado [a,†], Satomi Nadanaka [b,†], Yuko Naito-Matsui [b], Maria Iavazzo [c], Devin S. Brown [a], Marziyeh Hassanzadeh [a], Tuanjie Chang [a], Elena Polishchuk [c], Ingrid J. Pickering [d], Graham N. George [d], Mark J. Hackett [e], Nicola Volpi [f], Carmine Settembre [c,g], Hiroshi Kitagawa [b], B. Frank Eames [a,*]

[a] Department of Anatomy, Physiology, and Pharmacology, University of Saskatchewan, Saskatoon, SK, Canada
[b] Laboratory of Biochemistry, Kobe Pharmaceutical University, Higashinada-ku, Kobe, Japan
[c] Telethon Institute of Genetics and Medicine (TIGEM), Pozzuoli, Italy
[d] Department of Geological Sciences, University of Saskatchewan, Saskatoon, SK, Canada
[e] School of Molecular and Life Sciences (MLS), Curtin University, Perth, Australia
[f] Department of Life Sciences, University of Modena and Reggio Emilia, Modena, Italy
[g] Department of Clinical Medicine and Surgery, Federico II University, Naples, Italy

ARTICLE INFO

Keywords:
Endochondral ossification
Cartilage maturation
Chondroitin sulfate proteoglycans
XRF imaging
Endosulfatase
ARSI

ABSTRACT

During endochondral ossification, chondrocytes undergo maturation and biochemically modify the collagenous extracellular matrix of cartilage. Similar modifications to cartilage proteoglycans (PGs), which are predominantly chondroitin sulfate PGs, have not been characterized. Using synchrotron X-ray fluorescence imaging, we demonstrated that PG sulfation significantly decreased during cartilage maturation of chick embryos. Laser-capture microdissection and RNAseq revealed upregulation of Arylsulfatase I (*Arsi*) in mature cartilage of mouse. ARSI protein also increased in mature cartilage of mouse and chick *in vivo* and during maturation of ATDC5 chondrocytes *in vitro*, whereas expression of the two known chondroitin sulfate PG sulfatases (ARSB and GALNS) was not specific to mature cartilage. Colocalization studies suggested that ARSI is lysosomal, and lysosome homeostasis was altered in ARSI loss of function chondrocytes. Biochemical analyses of ARSI gain and loss of function cell lines and isolated cell-free systems revealed that ARSI is a novel chondroitin endosulfatase, specifically desulfating chondroitin-4-sulfate at pH 4.5. Finally, *Arsi* knockout in RCS chondrocytes caused increased expression of maturation genes, such as *Col10a1* and *Mmp13*. In total, these data identify ARSI as a novel PG sulfatase regulating endochondral ossification.

Introduction

During endochondral ossification of the growth plate, mesenchymal cells differentiate into chondrocytes and secrete an extracellular matrix (ECM) of collagens and proteoglycans (PGs) that serves as a cartilage template for subsequent bone formation [1]. Some of these chondrocytes undergo a developmental transition termed maturation, becoming hypertrophic and biochemically remodelling their collagenous ECM. While the initial cartilage template expresses abundant collagen type 2a1 (*Col2a1*), encoding the α1 chain of collagen II, mature chondrocytes downregulate *Col2a1* expression and upregulate collagen type 10a1 (*Col10a1*), encoding the α1 chain of collagen X [2]. Degradation of ECM molecules also occurs during cartilage maturation, because mature chondrocytes express collagen-degrading enzymes, such as matrix metalloproteinase 13 [3]. Biochemical modifications of PGs remain to be evaluated fully, but sulfation of glycosaminoglycans (GAGs) on the PG core protein (*i.e.*, PG sulfation) might be reduced during cartilage maturation [4–7].

While the PG synthesis pathway is well-known, several genes likely involved in reducing PG sulfation remain to be characterized. After PG core proteins are synthesized, a linker tetrasaccharide is added, and then repeating disaccharide GAG side chains extend from the linker [8,9].

* Corresponding author at: 2D01–107 Wiggins Road, Saskatoon, SK, S7N5E5, Canada.
E-mail address: b.frank@usask.ca (B.F. Eames).
† These authors contributed equally.

https://doi.org/10.1016/j.matbio.2026.03.005
Received 21 October 2025; Received in revised form 26 March 2026; Accepted 27 March 2026
Available online 29 March 2026
0945-053X/© 2026 The Authors. Published by Elsevier B.V. This is an open access article under the CC BY-NC license (http://creativecommons.org/licenses/by-nc/4.0/).

The repeating disaccharide of heparan sulfate GAGs is glucuronic acid (GlcA)/iduronic acid (IdoA) and *N*-acetyl glucosamine (GlcNAc), while chondroitin sulfate GAGs contain GlcA and *N*-acetyl galactosamine (GalNAc; [8]). Cartilage is predominantly comprised of chondroitin sulfate PGs (CSPGs; [10]). At this point in their synthesis, PGs get biochemically modified by the addition of *O*–linked sulfate esters at specific GAG residues. CSPGs may be sulfated on the 2-carbon of GlcA and the 4- and 6-carbons of GalNAc [11]. Specific sulfotransferases increase PG sulfation, and specific sulfatases reduce PG sulfation [12]. Among 17 sulfatases that have been identified in the human genome from gene sequence analyses [12], only two are known to specifically desulfate CSPGs. Arylsulfatase b (ARSB; S1_2 sulfatase subfamily) acts on chondroitin-4-sulfate (C4S), and GALNS (S1_5 sulfatase subfamily) acts on chondroitin-6-sulfate (C6S; [8,13,14]). Much must be learned about sulfatases, because the specific biochemical substrates of six putative sulfatases, including ARSI (S1_2 sulfatase subfamily), are not known [14,15].

PG sulfatases can be related functionally to lysosomes. Lysosomes are membrane-bound degradative organelles that contain hydrolytic enzymes that break down macromolecules such as proteins, lipids, carbohydrates, and nucleic acids into smaller components that can be reused [16]. Many sulfatases, such as ARSB, GNS, IDS, and GALNS, colocalize with lysosomes and play key roles in degradation of PGs [8]. ARSI has no known cellular localization [15]. A relationship between sulfatase function and lysosome biogenesis has been established. Genetic mutations in lysosomal sulfatases lead to inherited metabolic diseases known as mucopolysaccharidosis (MPS), characterized by lysosomal accumulation (storage) of undegraded PG molecules [17]. Cellular homeostasis of lysosomes, including numbers and sizes, is altered in MPS [16].

PG sulfation influences cartilage function and can affect endochondral ossification [18–20]. The negative charge of PG sulfation attracts more water, increasing the compressive-resistant strength of cartilage [21]. Inadequate PG sulfation can cause a variety of skeletal defects during development. Mice with mutations in either *Papss2* (regulates the sulfate donor within the cell), *Slc26a2* (transports sulfate within the cell), or *Sumf1* (activates sulfatases) have reduced chondrocyte proliferation, severe growth retardation, and delayed secondary ossification center formation [22–25]. In human patients, mutations to *ARSB* or *GALNS* can cause MPS types VI or IVA, respectively [26]. Both MPS IVA and VI cause reduced growth of bones that form by endochondral ossification, but the underlying cellular and molecular mechanisms are currently unknown [27,28].

Given the relevance of PG sulfatases to human disease, the biochemical functions of the remaining orphan sulfatases need to be revealed. Initially, we used synchrotron-based X-ray fluorescence (XRF) imaging to reveal that PG sulfation significantly decreases during cartilage maturation. Supporting the hypothesis that a chondroitin sulfatase was expressed during cartilage maturation, laser-capture microdissection/RNAseq and other studies demonstrated that expression of ARSI, but not ARSB nor GALNS, increased as sulfate esters decreased in developing mature cartilage. Gain- and loss-of-function studies *in vitro* revealed that ARSI is a novel, lysosomal chondroitin endosulfatase that regulates lysosome homeostasis and maturation genes in chondrocytes, opening the pathway for understanding how biochemical modification of PGs affects endochondral ossification.

Results

PG sulfation decreased during cartilage maturation

Levels of PG sulfation were measured during cartilage maturation of the HH36 chick humerus, which undergoes endochondral ossification. Mature cartilage regions were identified using histological and

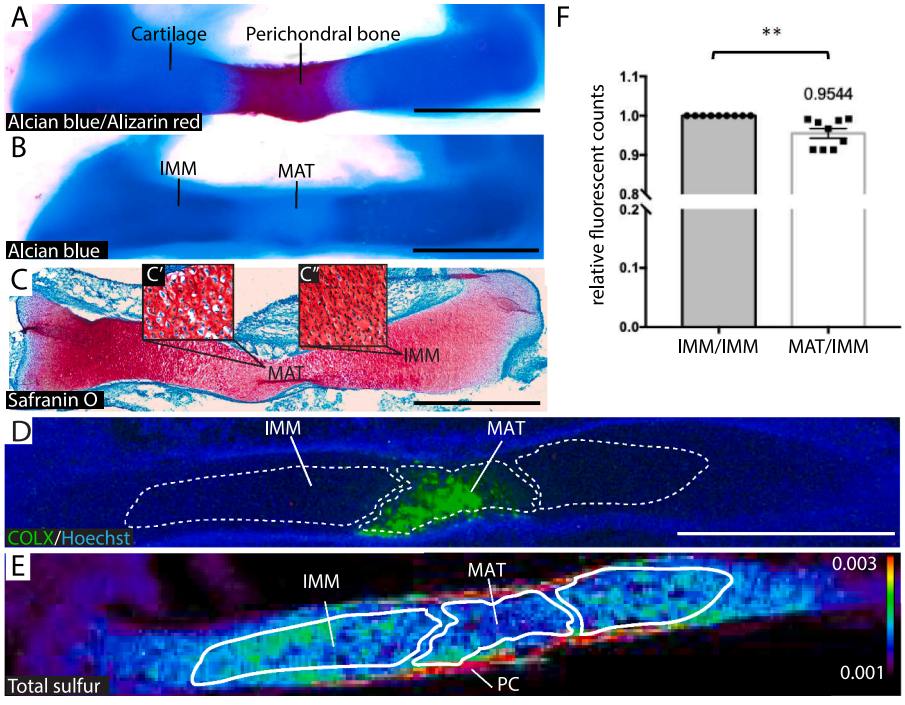

Fig. 1. Sulfation decreased during cartilage maturation of the HH36 chick humerus. (A) Whole-mount Alcian blue and Alizarin red staining indicated cartilage and perichondral bone regions, respectively. (B) Whole-mount Alcian blue appeared decreased in mature cartilage (MAT) underlying perichondral bone, compared to immature cartilage (IMM). (C) Similarly, Safranin O staining of sections appeared decreased in mature cartilage and showed hypertrophic chondrocytes in MAT (C') and non-hypertrophic chondrocytes in IMM (C''). (D) COLX expression verified MAT on sections and was used to define MAT and IMM regions (white dashed lines) for XRF image analysis. (E) XRF imaging of adjacent sections suggested that total sulfur levels decreased in MAT. (F) Quantitation of XRF images (n = 9) and one-sample t-test revealed a significant decrease of 4.5 ± 1.2 % in the average total sulfur in MAT, relative to IMM. $^{**}p < 0.005$. Abbreviations: IMM=immature cartilage; MAT=mature cartilage; PC=perichondrium. Scale bars: A-D = 1 mm.

molecular analyses. Whole-mount Alizarin red staining, which binds mineralized tissue, revealed perichondral bone in the mid-diaphysis (Fig. 1A). Whole-mount staining of Alcian blue, which binds sulfated PGs, appeared reduced in the cartilage region that is directly underneath perichondral bone (Fig. 1B). Similarly, reduced staining levels of Safranin O, which also binds sulfated PGs, on histological sections of the HH36 chick humerus were apparent in this cartilage region, which was confirmed as mature cartilage by the presence of hypertrophic chondrocytes and expression of Collagen type X (COLX; Fig. 1C',C'',D; [2]).

Synchrotron-based XRF imaging of sections of the HH36 chick humerus revealed that sulfur was enriched in cartilage, relative to surrounding tissues (n = 9; Fig. 1E), as previously reported [6]. To quantitate and compare each cartilage region's sulfur levels, COLX immunostaining on adjacent sections was used to define mature cartilage, as well as nearby immature cartilage (Fig. 1D, dotted lines). Qualitatively, COLX immunostained regions mostly fit well within a low sulfur region (Fig. 1E). Quantitation of sulfur levels in these identified regions verified a significant decrease (4.5 ± 1.2 %) in the average total sulfur content in mature cartilage compared to immature cartilage (Fig. 1F). The resting and proliferative zones in the extreme epiphyses of developing cartilage also appeared to have lower levels of total sulfur, although this was not quantitated.

A diversity of chemical forms of sulfur are present in biological tissues like cartilage, but PG sulfation is reflected specifically by sulfate esters [6,29]. To investigate relative levels of specific chemical forms of sulfur in developing immature and mature cartilage, X-ray absorption near edge structure (XANES) analysis was performed on HH36 chick humerus sections. Combined fittings of five sulfur chemical forms from standard curve measures (among eight tested) matched very well the averaged XANES spot scans (n = 4; Supplemental Fig. S1). *O*-linked sulfate esters were the most abundant (77.3 ± 2.1 % of sulfur in immature cartilage; 69.5 % ± 10.7 % in mature cartilage), followed by sulfonic acids, thioethers, disulfides, and sulfoxides (Table 1). *N*-linked sulfate esters were practically negligible in developing cartilage and were not included in the final XANES fitting, as reported previously [6]. The fact that *O*-linked sulfate esters were the most abundant form of sulfur detected by XANES in developing chick cartilage suggested that the majority of sulfur detected by XRF was from PGs.

To visualize the distribution of different chemical forms of sulfur in developing cartilage *in situ*, chemically specific XRF maps were generated (n = 5). COLX immunostaining on adjacent sections was used to define the mature and nearby immature cartilage regions (dotted lines, Fig. 2A). Qualitatively, the relative intensities of total sulfur and sulfate esters had similar distributions in the HH36 chick humerus, with lower levels apparent in the mature cartilage region (Fig. 2B,C). The similarity in maps of total sulfur and sulfate esters detected by chemically-specific XRF supported XANES results that PG sulfation accounted for the majority of sulfur in cartilage. By contrast, maps of sulfonic acid and lower oxidation states of sulfur did not clearly follow this distribution pattern across developing cartilage (Fig. 2D,E). Quantitation of chemically specific XRF maps revealed that sulfate esters decreased significantly (13.4 ± 4.1 %) in mature cartilage, compared to immature cartilage (Fig. 2F). Total sulfur also tended to decrease (8.8 ± 4.2 %) in mature cartilage, but not significantly in these samples (Fig. 2F). Like the XANES analyses (Table 1), sulfonic acids tended to increase slightly in mature cartilage (25.4 ± 35 %), but not significantly, likely due to large variation between samples (Fig. 2F). In summary, significant decreases in *O*-linked sulfate esters demonstrated that PG sulfation decreases during cartilage maturation.

Table 1
XANES measures (n = 4) revealed that *O*-linked sulfate esters were the majority of sulfur forms in the HH36 chick humerus.

	Immature	Mature
O-linked sulfate esters	77.3 % ± 2.1 %	69.5 % ± 10.7 %
Sulfonic acids (taurine)	13.6 % ± 2.0 %	22.0 % ± 10.5 %
Thioethers	7.1 % ± 1.0 %	5.5 % ± 1.5 %
Disulfides	1.1 % ± 0.1 %	2.0 % ± 0.9 %
Sulfoxides	0.9 % ± 0.2 %	1.0 % ± 0.4 %

Since loss of PG sulfation is linked to PG degradation [24,25], overall loss of PGs during cartilage maturation was investigated using Fourier transform infrared (FTIR) imaging on sections of the HH36 chick humerus (n = 7; Supplemental Methods). Using previously-reported wave numbers, proteins (Amide I: 1590–1720cm^{-1}; [30]) tended to decrease in mature cartilage (5 ± 3 %), compared to immature cartilage, although this was not statistically significant (Supplemental Fig. S2B,E). Since proteins were somewhat decreased, PG and GAG FTIR maps were normalized to the integrated Amide I peak. With or without this normalization, PGs (985–1140cm^{-1}; [31]) and GAGs (second derivative peak 1374cm^{-1}; [32]) also both tended to decrease in mature cartilage (4 ± 4 % and 3 ± 3 %, respectively), but not significantly (Supplemental Fig. S2C-E). These FTIR imaging data suggested that at least some of the sulfate esters in mature cartilage decreased independently of overall PG levels.

ARSI, but not GALNS or ARSB, was expressed specifically in mature cartilage in mouse and chick

To test the hypothesis that the significant decrease in PG sulfation during cartilage maturation was due to a PG sulfatase expressed specifically in mature cartilage, our published transcriptomic dataset [33] from laser capture microdissected mature and immature cartilage (n = 3 for each tissue) in the E14.5 mouse humerus was analyzed. *Galns* and *Arsb* encode the only known animal sulfatases that specifically remove sulfate esters from CSPGs, the main PG in cartilage matrix [8]. However, neither *Galns* nor *Arsb* transcripts were increased in mature cartilage (Table 2). Genes encoding known heparan sulfate PG sulfatases, such as *Gns, Ids, Arsg,* and *Sulf1* [8], also were not enriched in mature cartilage; *Sulf2* was even significantly downregulated (Table 2). Of the putative PG sulfatases, including *Arsd, Arse, Arsf, Arsh, Arsi,* and *Arsj*, only *Arsi* was significantly increased (1.65 $\log_2$FC) in mature over immature cartilage (Table 2). The classic maturation marker *Col10a1* was also enriched (10.62 $\log_2$FC) in mature cartilage in these datasets (Table 2). In summary, transcriptomic analyses identified that the gene *Arsi*, encoding an orphan sulfatase, was specifically expressed during cartilage maturation.

To verify that analyses in different species did not confound these results, ARSI sequence conservation was evaluated, and ARSI expression was analyzed in both chick and mouse. ARSI protein sequence was highly conserved across vertebrates, even more so when comparing just the putative sulfatase domain, suggesting functional conservation (Table 3, Supplemental Fig. S3, Supplemental Table 1). The sulfatase domain of human ARSI was 97.4 % similar with *Mus musculus*, 90.0 % with *Gallus gallus*, 75.3 % with *Danio rerio* Arsia, and 74.7 % with *Danio rerio* Arsib (zebrafish retained duplicate copies of ARSI after the teleost genome duplication; [34]).

To analyze ARSI expression in chick cartilage, RNA *in situ* hybridization was performed (Supplemental Methods). *ARSI* mRNA expression was confirmed in mature cartilage of the HH36 chick humerus (n = 3), in similar domains as the prehypertrophic marker *IHH*, but restricted to superficial regions of the cartilage (Supplemental Fig. S4A-B'). *ARSI* was not expressed in more mature regions of mature cartilage, such as where *COL10A1* or *SPP1* were expressed, or where *COL2A1* was downregulated (Supplemental Fig. S4C-E'). These expression results were confirmed with two other probes targeting different portions of the *ARSI* mRNA (data not shown). Transcripts for the chondroitin sulfatase genes *GALNS* and *ARSB* did not show any specific expression in immature or mature cartilage domains of the HH36 chick humerus (Supplemental Fig. S4F-G').

Immunostaining was used to further confirm expression of ARSI in mature cartilage of the chick. In the HH36 chick humerus (n = 10),

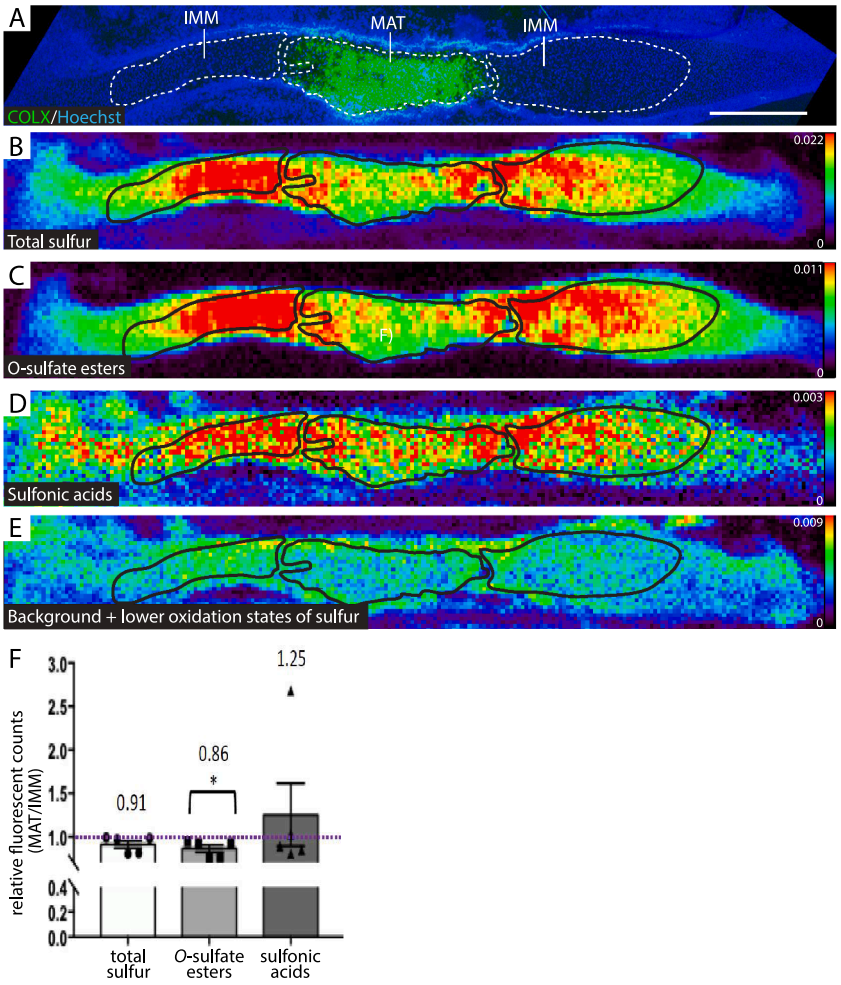

Fig. 2. Chemically specific XRF maps of the HH36 chick humerus revealed a significant decrease in *O*-sulfate esters in mature cartilage. (A) COLX immunohistochemistry defined mature (MAT) and nearby immature (IMM) cartilage regions of interest (dotted lines). Levels of total sulfur (B) and *O*-sulfate esters (C) had similar distributions across developing cartilage, with lower levels in MAT. Levels of sulfonic acid (D) and lower oxidation states of sulfur (E) did not follow a clear distribution pattern across developing cartilage. (F) Quantitation of MAT and IMM (black outlines in B-E) on XRF images ($n = 5$) showed that *O*-sulfate esters significantly decreased 13.4 ± 4.1 % in MAT. *$p < 0.003$. Abbreviations: IMM=immature cartilage; MAT=mature cartilage. Scale bar=1 mm.

Table 2
The putative PG sulfatase *ARSI* was the only sulfatase significantly increased in mature cartilage of the E14.5 mouse humerus ($n = 3$).

	immature cartilage	mature cartilage	log_2FC	p value
Arsb	25 ± 20	37 ± 51	0.57	0.72
Arsg	22 ± 12	26 ± 4	0.24	0.60
Arsi	371 ± 179	1162 ± 134	1.65	*0.004*
Galns	103 ± 1	118 ± 42	0.20	0.56
Gns	406 ± 86	430 ± 165	0.08	0.84
Ids	238 ± 159	210 ± 146	−0.18	0.83
Sulf1	1364 ± 1195	883 ± 459	−0.63	0.55
Sulf2	2150 ± 554	541 ± 167	−1.99	*0.009*
Col10a1	9 ± 1	14,174 ± 3213	10.62	*0.002*

hypertrophic chondrocytes and COLX expression on adjacent sections were again used to estimate the region of mature cartilage (Fig. 3A,B; dotted lines in all panels). ARSI was restricted to mature cartilage, but dual immunostaining with COLX confirmed that ARSI protein was in the hypertrophic domain of mature cartilage (Fig. 3C,D). COLX immunoreactivity was in the extracellular matrix, but ARSI immunoreactivity did not overlap with COLX, appearing closer to nuclei, suggesting intracellular localization (Fig. 3B-D'). Similar to mRNA expression, ARSI protein was expressed in more superficial regions of mature cartilage (Supplemental Fig. S5). Neither of the two known CSPG sulfatases,

Table 3
Amino acid sequences of the putative sulfatase domain of ARSI were highly conserved across vertebrate clades. Numbers reflect % identity. Abbreviations: (a)=Arsia; (b)=Arsib; *Dre=Danio rerio; Gga=Gallus gallus; Hsa=Homo sapiens; Mmu=Mus musculus.*

	Hsa	*Mmu*	*Gga*	*Dre* (a)	*Dre* (b)
Hsa	100	97.4	90.0	75.3	74.7
Mmu		100	90.4	68.2	66.4
Gga			100	70.6	66.7
***Dre* (a)**				100	71.3
***Dre* (b)**					100

GALNS and ARSB, showed increased expression in mature cartilage (Fig. 3E,F). GALNS was not above background levels in any region of the humerus. ARSB was expressed at similar levels in both mature and immature cartilage regions, with apparent intracellular immunoreactivity (Fig. 3F').

To further investigate conservation of ARSI expression during chondrocyte maturation, immunostaining of the E14.5 mouse humerus and a mouse chondrocyte cell line, ATDC5 (Supplemental Methods), were performed. Indeed, ARSI and COLX immunostaining were in similar domains of mature cartilage in the E14.5 mouse humerus (Supplemental Fig. S6A,B). Cartilage differentiation in micromasses of

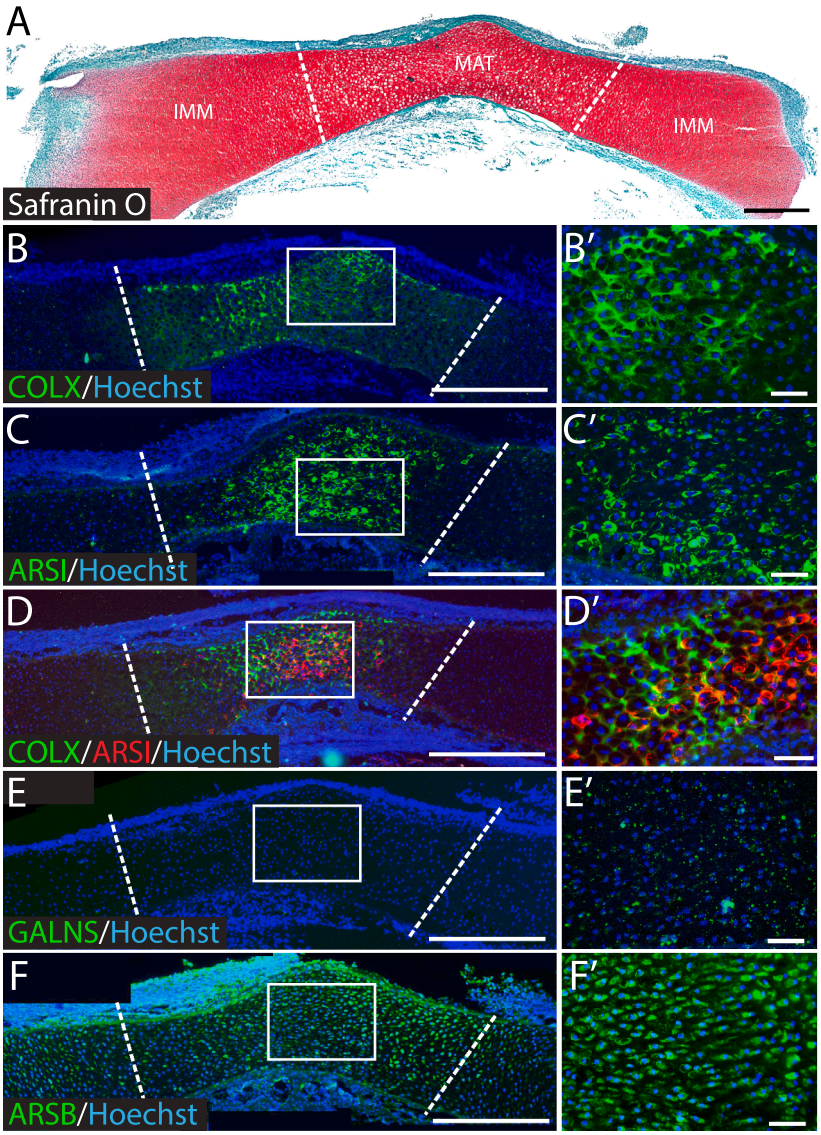

Fig. 3. Immunostaining demonstrated that ARSI, but not GALNS or ARSB, was specifically expressed in mature cartilage of the HH36 chick humerus. (A) Safranin O staining showed hypertrophic chondrocytes in mature cartilage (dotted lines in all panels estimate the mature cartilage region). In addition to COLX (B), ARSI (C) was expressed in mature cartilage ($n = 10$). (D) Dual immunostaining for COLX (green) and ARSI (red) confirmed their expression in mature cartilage, but also suggested that ARSI was expressed intracellularly. In both regions of the humerus, GALNS (E) was not observed above background levels, while ARSB (F) was observed in similar levels. Boxed regions in panels A-F indicate regions shown in panels A'-F', respectively. Abbreviations: IMM=immature cartilage, MAT=mature cartilage. Scale bars: A-*F* = 400μm; A'-F'=50μm.

ATDC5 cells was confirmed by Alcian blue staining, and increased COLX immunostaining was apparent during ATDC5 chondrocyte maturation (Supplemental . S6C—H). Immunostaining and Western blot analyses also showed that ARSI levels increased during ATDC5 chondrocyte maturation (Supplemental Fig. S6I-L). In sum, these *in vitro* and *in vivo* protein expression data confirmed transcript data in chick and mouse, demonstrating conserved, specific expression of ARSI in mature cartilage, where XRF imaging showed that PG sulfation was decreased.

ARSI colocalized with lysosomes and functionally impacted lysosome homeostasis

To confirm immunostaining results suggesting that ARSI was localized intracellularly, and to identify its cellular compartments, imaging was undertaken of cells stably expressing fluorescent-tagged human ARSI. Human ARSI with EGFP fused to its C-terminus was expressed in HeLa cells (Fig. 4A). Dual immunostaining revealed that ARSI was colocalized with the lysosome marker LAMP1 and the endosome marker RAB5 (Fig. 4B-G'; [35]), suggesting that ARSI is a bona fide lysosomal enzyme.

To evaluate the impact of ARSI on lysosome homeostasis, *Arsi* loss of function was created in the RCS line of rat chondrocytes, and lysosome numbers and sizes were analyzed. CRISPR targetting of *Arsi* was confirmed by Western blotting of two independent clones, both of which had a lack of ARSI protein expression (Fig. 5A). Three independent quantitative measures of lysosomes were performed. FACS analyses of RCS chondrocytes labelled with the vital dye LysoTracker demonstrated that fluorescence intensity was significantly increased in two *Arsi*$^{-/-}$ chondrocyte clones, compared to a parental control clone (Fig. 5B). Those two *Arsi*$^{-/-}$ clones also had significant increases in lysosome numbers, compared to a parental control, upon quantitation of immunostaining with LAMP1 (Fig. 5C-F). Finally, quantitation in TEM images of one the *Arsi*$^{-/-}$ clones showed significantly larger lysosomes, compared to a parental clone (Fig. 5G-I). In total, these data revealed

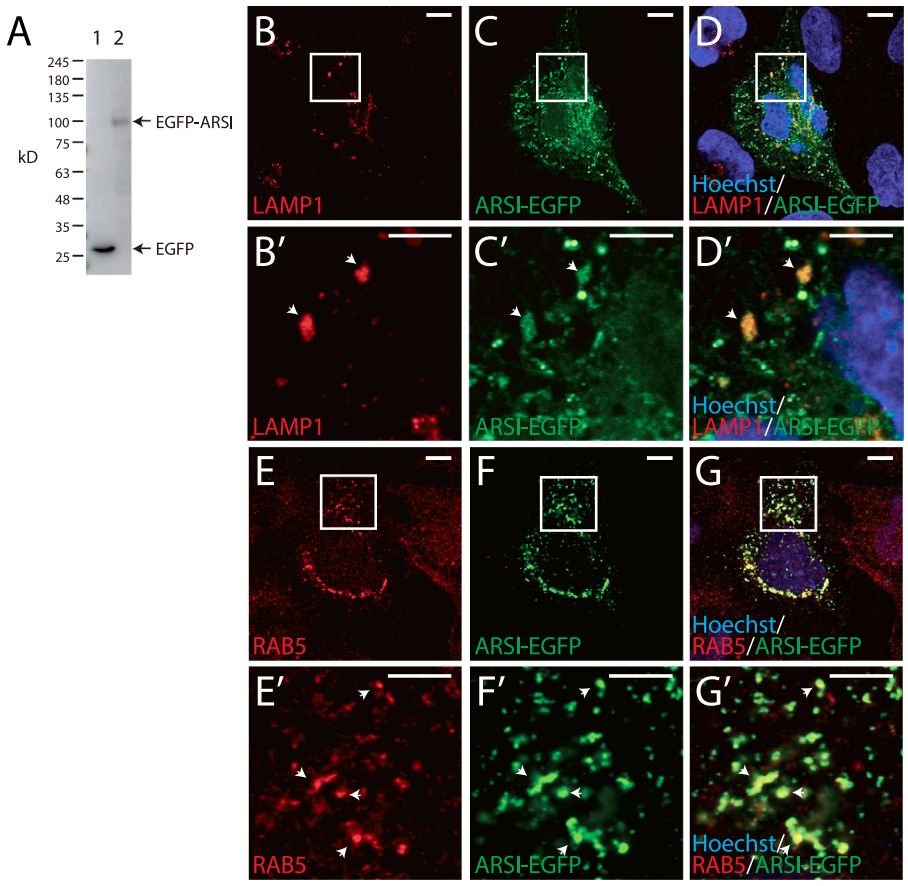

Fig. 4. EGFP-tagged ARSI colocalized with lysosomes and endosomes in HeLa cells. (A) Anti-GFP Western blot demonstrated expression of EGFP (lane 1) EGFP-tagged human ARSI (Lane 2) in HeLa cells 2 days after transfection. Immunostaining showed colocalization (white arrowheads) of LAMP1 and ARSI (B-D) and colocalization of RAB5 and ARSI (E-G) in HeLa cells. Anti-GFP was used for immunostaining of ARSI. Boxed regions in panels B-G indicate regions shown in panels B'-G', respectively. Scale bars: B-*G* = 10μm; B'-G'=5μm.

that ARSI is lysosomal and regulates lysosome homeostasis.

ARSI is a novel endosulfatase of chondroitin-4-sulfate (C4S)

To determine the biochemical activity of the orphan sulfatase ARSI *in vitro*, human *ARSI* was overexpressed in HeLa cells. RT-qPCR showed that HeLa cell clones transfected with an empty vector expressed *ARSI* at very low levels ($n = 6$; $n = 3$ from each of 2 clones), while *ARSI* was successfully overexpressed in *ARSI*-transfected HeLa cell clones ($n = 9$; $n = 3$ from each of 3 clones; Fig. 6A). HPLC analyses of harvested CS disaccharides demonstrated that total CS amounts were significantly reduced in stable *ARSI*-transfected HeLa clones ($n = 9$; $n = 3$ from each of 3 clones), compared to stable empty vector-transfected control clones ($n = 6$; $n = 3$ from each of 2 clones; Fig. 6B). *ARSI* expression caused the ratio of C4S to total CS to significantly decrease, while the ratio of non-sulfated C0S to total CS significantly increased (Fig. 6C). Arguing against any complication from genetic compensation in this overexpression experiment, *ARSI*-transfected HeLa clones did not alter the expression of genes that promote CS sulfation, such as the sulfotransferases *CHST3, CHST11*, and *CHST12*, or the glucuronyltransferase *B3GAT3*, compared to empty vector-transfected HeLa clones (Fig. 6D).

To further evaluate ARSI sulfatase activity, RCS *Arsi*$^{-/-}$ chondrocyte clones underwent HPLC analyses ($n = 3$). The percentage of C4S significantly increased in RCS *Arsi*$^{-/-}$ chondrocyte clones (Fig. 7), producing a significant increase of the overall charge density from 0.79 to 0.88. Meanwhile, the non-sulfated C0S significantly decreased, and no changes to the other disaccharides sulfated in different positions were observed (Fig. 7). *Chst11* expression was not significantly changed in *Arsi*$^{-/-}$ chondrocytes (Supplemental Fig. S7), suggesting that gene compensation did not underlie differences in sulfated GAG composition.

To estimate specific activity of ARSI on CS sugars, human *ARSI* was purified from HeLa cells using a Protein A tag and incubated with the monosaccharide GalNAc4S or GalNAc6S. Because ARSI was overexpressed in mammalian cells, endogenous SUMF1 might not be sufficient, leading to the production of immature (non-formylglycine-modified) ARSI. To address this, a co-expression system for ARSI and SUMF1 enhanced the maturation efficiency, ensuring sufficient specific activity of ARSI for further analyses. A twelve-hour incubation of GalNAc4S in 25 mM sodium acetate (pH4.5) with 410 ng of Protein A-fused ARSI expressed in the presence of SUMF1 gave rise to 0.5 nmol of GalNAc (Supplemental Fig. S8). Thus, the specific activity on GalNAc4S of protein A-fused ARSI was estimated to be 0.1 nmol/μg/hr. No activity of ARSI was detected on GalNAc6S in this assay, nor was activity detected at pH6.5 (Supplemental Fig. S8).

The relatively low reactivity of ARSI toward the monosaccharide GalNAc4S suggested that the monosaccharide system might not fully represent the enzyme's physiological function. Therefore, activity of ARSI on polymeric C4S and C6S were tested using the same cell-free biochemical system above, but with ARSI and SUMF1 co-expression in COS-7 cells ($n = 3$, each experimental group; Fig. 8A,B). These biochemical analyses at pH4.5 revealed a significant reduction in 4-*O*-sulfated disaccharide units (ΔDi-4S), accompanied by a corresponding increase in non-sulfated disaccharide units (ΔDi-0S; Fig. 8C). No such activity was detected on C4S at pH6.5, nor on C6S at either pH4.5 or pH6.5 (Fig. 8C,D). According to the manufacturer's specifications, the molecular weight of the substrate (CS-A) used in this study ranges from

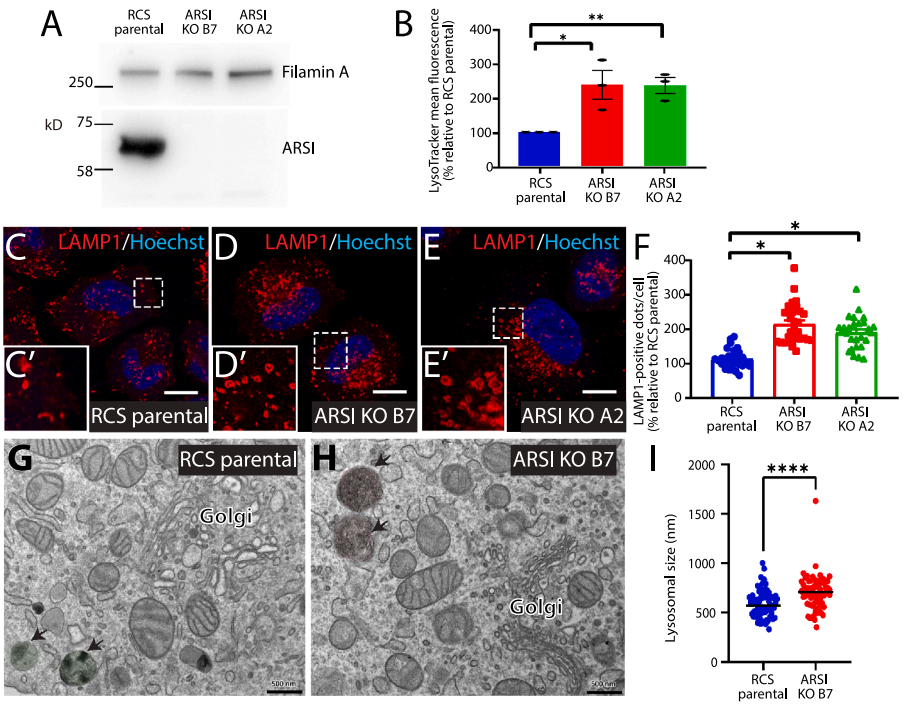

Fig. 5. ARSI inhibited lysosome number and size in RCS chondrocytes. (A) Western blot confirmed loss of ARSI protein in two CRISPR-targetted RCS chondrocyte clones. Filamin A was used as a loading control. (B) FACS analysis labeled with LysoTracker and Hoechst dyes revealed that two ARSI knockout (KO) RCS chondrocyte clones had increased lysosomes per cell, compared to parental control ($n = 3$, each clone). (C-F) Immunostaining of LAMP1 (red) with Hoechst dye (blue) in clones of parental (C) and two ARSI knockout (D,E) RCS chondrocytes demonstrated increased lysosomes, which was confirmed by quantification of LAMP1-positive dots/cell ($n = 3$, each clone). Dashed boxed regions in panels C-E indicate regions shown in panels C'-E'. (G-I) TEM images of RCS chondrocytes also showed smaller lysosomes in a parental clone (G), compared to an ARSI knockout clone (H), which was verified by quantitation (I). Arrows indicate lysosomes. *$p < 0.05$; **$p < 0.005$; ****$p < 0.0005$. Abbreviation: KO=knockout. Scale bars: C-E = 11 μm; G,H = 500 nm.

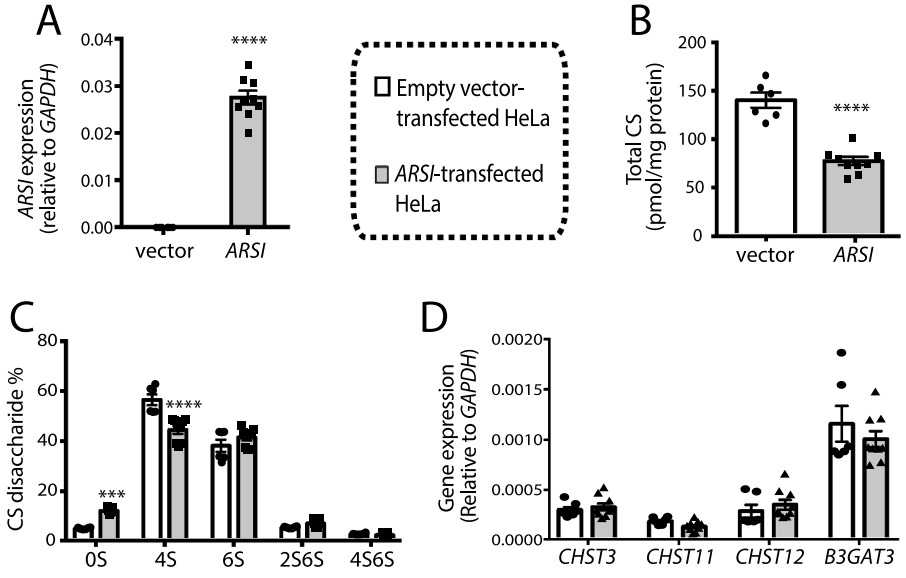

Fig. 6. *ARSI* overexpression in HeLa cells reduced sulfation of CS GAGs. (A) RT-qPCR showed that human *ARSI* was successfully overexpressed in transfected HeLa cells. (B) HPLC demonstrated a decrease in total CS in *ARSI*-transfected HeLa clones, compared with empty vector controls. (C) The ratio of 4S to total CS decreased, while the ratio of non-sulfated 0S increased. (D) RT-qPCR revealed that the expression of enzymes that promote CS sulfation, like *CHST3, CHST11,* and *CHST12,* and the glucuronyltransferase *B3GAT3* were not affected. ***$p < 0.0002$; ****$p < 0.0001$. Abbreviations: 0S=non sulfated chondroitin, 2S=2-sulfated chondroitin, 4S=4-sulfated chondroitin, 6S=6-sulfated chondroitin.

25,000 to 50,000. Given that the molecular weight of a monosulfated disaccharide unit is 461, each CS-A chain is estimated to consist of approximately 54 to 108 disaccharide units. In this structural context, the disaccharide units located at the non-reducing termini account for only 1–2 % of the total disaccharides. In our experimental results, however, the reduction rate of 4-sulfated disaccharides (ΔDi-4S) upon ARSI treatment reached 10 % compared to the empty vector control. This reduction significantly exceeds the theoretical limit (1–2 %) expected if the reaction occurred exclusively at the chain termini. In total, these gain- and loss-of-function biochemical data revealed that ARSI is a

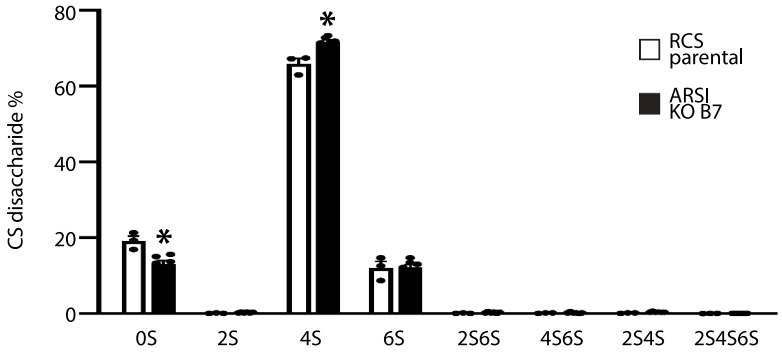

Fig. 7. ARSI knockout in RCS chondrocytes increased sulfation of C4S. HPLC analyses ($n = 3$, each group) demonstrated that the loss of ARSI in RCS chondrocytes caused the percentage of C4S to significantly increase, while the percentage of non-sulfated CS significantly decreased. *$p < 0.05$. Abbreviation: KO=knockout.

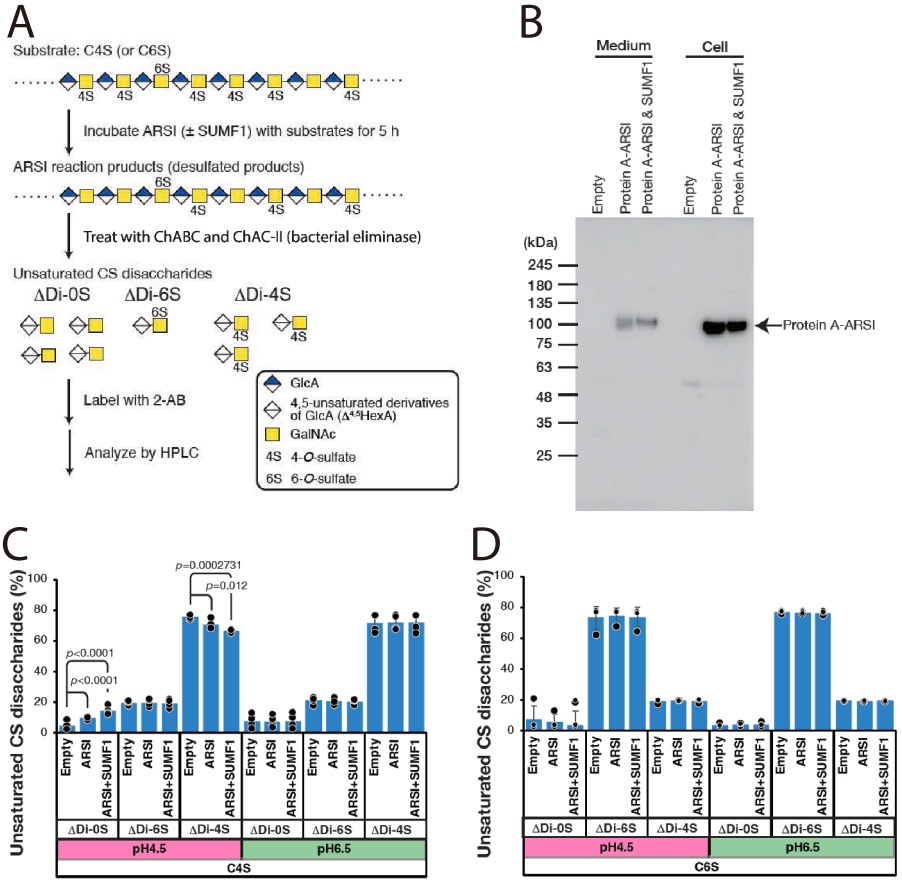

Fig. 8. ARSI has endosulfatase activity on C4S, but not on C6S, at acidic pH. (A) Schematic representation of the enzymatic assay. Chondroitin 4-sulfate (C4S) or chondroitin 6-sulfate (C6S) was used as the substrate. Recombinant ARSI, expressed either alone or co-expressed with SUMF1 in COS-7 cells, was incubated with the substrate for 5 h at pH 4.5. The resulting products were subsequently digested into unsaturated CS disaccharides by ChABC and ChAC-II, and the enzymatic desulfation activity of ARSI was evaluated by analyzing the liberated unsaturated disaccharides using HPLC. (B) COS-7 cells were transfected with either an empty vector, a Protein A-fused ARSI expression vector, or a combination of Protein A-fused ARSI and SUMF1 expression vectors. After 2 days of incubation, ARSI was purified from the culture medium and cell lysates using IgG-Sepharose. The amount of the purified ARSI used in the enzymatic assays were confirmed by SDS-PAGE and western blotting. (C) Enzymatic reactions were performed using C4S or C6S as substrates at pH 4.5 or pH 6.5 using recombinant ARSI isolated from the cell lysates. The resulting products were digested into unsaturated disaccharides with chondroitinase ABC and analyzed by HPLC. The percentage of the resulting unsaturated disaccharide units (ΔDi-0S, ΔDi-4S, and ΔDi-6S) was determined. Data are presented as individual data points, the mean, and the standard deviation from four independent experiments ($n = 4$).

novel chondroitin endosulfatase, targeting internal 4-*O*-sulfate groups of CS/DS chains under acidic conditions, although ARSI can also act on the nonreducing terminal GalNAc4S.

ARSI inhibited chondrocyte maturation in vitro

RCS chondrocytes can model chondrocyte maturation *in vitro* by

treatment with fibroblast growth factor (FGF; [36]). To evaluate if ARSI regulates chondrocyte maturation, RCS *Arsi*$^{-/-}$ chondrocytes were stimulated to undergo maturation by addition of FGF18, and maturation markers were analyzed by RT-qPCR. Right before FGF18 treatment, *Arsi*$^{-/-}$ chondrocytes already had significantly increased expression of the maturation markers *Mmp13* and *Vegfa*, compared to parental chondrocytes (Fig. 9). They also had significantly increased *Col2a1* expression. In parental RCS chondrocytes, FGF18 treatment for 24 h caused significant increases in the maturation markers *Mmp13* and *Vegfa*, compared to parental cells before treatment, verifying FGF18 induced chondrocyte maturation (Fig. 9). In *Arsi*$^{-/-}$ chondrocytes, the maturation marker *Mmp13* significantly increased after FGF18 treatment, compared to *Arsi*$^{-/-}$ chondrocytes before FGF18 addition (Fig. 9). *Col2a1* is known to be down-regulated during chondrocyte maturation [37], and *Arsi*$^{-/-}$ chondrocytes had significantly decreased expression of *Col2a1* after FGF18 treatment.

Comparing parental and *Arsi*$^{-/-}$ chondrocytes after FGF18 induction of maturation, important differences were observed. *Arsi*$^{-/-}$ chondrocytes expressed the maturation markers *Col10a1* and *Mmp13* significantly higher than FGF-treated parental chondrocytes (Fig. 9). Also, *Arsi*$^{-/-}$ chondrocytes had significantly decreased expression of *Col2a1* after FGF18 treatment, compared to parental RCS cells (Fig. 9). These *in vitro* data showed that ARSI normally inhibits chondrocyte maturation, since maturation markers were significantly increased in *Arsi*$^{-/-}$ chondrocytes.

Discussion

Modifications to the ECM of the developing growth plate during endochondral ossification has focused on collagens [3], but similar changes to PGs have not been fully characterized [4–7]. Here, we used synchrotron imaging to illustrate for the first time that *O*-linked sulfate esters, reflecting PG sulfation, decreased significantly during cartilage maturation in developing long bones. Interestingly, the orphan sulfatase ARSI was differentially expressed in this same region, while the known chondroitin sulfatases ARSB and GALNS were not. Following this lead, we revealed the first biochemical characterization of ARSI as a lysosomal CSPG endosulfatase, specifically targetting internal 4-*O*-sulfate groups of CS/DS at acidic pH. Our results supplement the scarce literature about ARSI and potentiate future work uncovering its role in skeletal development and disease.

ARSI was identified decades ago as an arylsulfatase through bioinformatic analysis, but many questions about its biochemical and biological roles remain to be unveiled [12]. General sulfatase activity of ARSI was described using the artificial substrate 4-methylumbelliferyl sulfate [38], but its biological substrate remained elusive. ARSI might have been predicted to function like ARSB, whose substrate is GalNAc4S, because they have high sequence similarity [12,39]. Indeed, experiments here confirmed that ARSI is a novel CSPG endosulfatase. Overexpression of ARSI in HeLa cells significantly decreased the relative levels of GalNAc4S, while knockout of ARSI in RCS chondrocytes significantly increased relative levels of GalNAc4S. Importantly, in a cell-free system, ARSI showed specific activity on GalNAc4S (0.1 nmol/μg/hr), but not on GalNAc6S. Additional experiments showed a high affinity for ARSI on polymeric CS. While the CS-A substrate used in this study contains approximately 20 % CS-C (ΔDi-6S) and only trace levels of CS-D (ΔDi-diSD), we cannot exclude the possibility that these neighboring sulfation patterns influence the desulfation efficiency of ARSI. Further investigations using chemically synthesized oligosaccharides with defined and uniform sulfation patterns will be required to strictly define the substrate specificity and the structural requirements for ARSI activity. We speculate that ARSI's substrate specificity is strictly governed by the uronic acid component (GlcA *vs.* IdoA), but ARSI may also function as an auxiliary endo/exosulfatase in the DS degradation process. While our data indicate a preference for internal 4-*O*-sulfate groups, under specific physiological conditions, ARSI may facilitate the desulfation of GalNAc4S residues exposed at the non-reducing end after the sequential actions of iduronate-2-sulfatase and iduronidase. Future experiments should test the reaction efficiency of ARSI toward polymeric DS, compared to GlcA-containing CS.

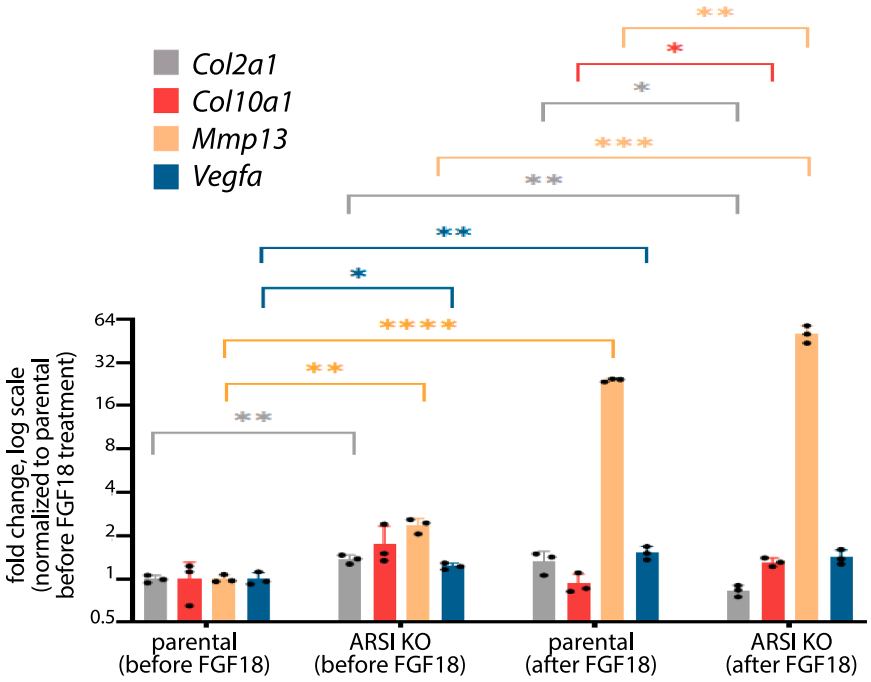

Fig. 9. ARSI inhibited chondrocyte maturation *in vitro*. RT-qPCR revealed that *Arsi*$^{-/-}$ RCS chondrocytes had significantly increased expression of *Col2a1* and the maturation markers *Vegfa* and *Mmp13*, compared to parental chondrocytes ($n = 3$). After induction of maturation by FGF18 for 24 h, *Arsi*$^{-/-}$ chondrocytes expressed the maturation markers *Col10a1* and *Mmp13* significantly higher than FGF-treated parental chondrocytes, also with significantly decreased *Col2a1* ($n = 3$). *$p < 0.05$; **$p < 0.01$; ***$p < 0.001$; ****$p < 0.0001$. Abbreviations: KO=knockout.

Why have two chondroitin 4-*O*-sulfatases? One answer is that ARSI has endosulfatase activity, while ARSB is exclusively an exosulfatase, so they can target different regions of the polymeric GAG. Spatial restriction of activity might also answer this question. As an example, SULF1 and SULF2 have redundant biochemical specificity for removing 6-*O*-sulfates from heparan sulfate PGs [40]. However, their expression patterns in the body are different, and thus, loss of *Sulf1* has a different phenotype from loss of *Sulf2* [41]. Similarly, ARSB and ARSI might both have specificity for C4S, but our extensive expression analyses (*i.e.*, RNA sequencing, RNA *in situ* hybridization, and immunofluorescence) showed that their expression patterns are different. In developing cartilage of both mouse (E14.5) and chick (HH36), ARSI, but not ARSB, was specifically expressed in mature cartilage, expanding upon a previous report [42]. Within cartilage, aggrecan is the major PG of the ECM, but ARSI might also act on GAGs of decorin or biglycan. Mouse genetic models suggest that some *Arsb*$^{-/-}$ bone phenotypes can be rescued by enzyme replacement therapies in osteoclasts and osteocytes, not chondrocytes [43,44]. Considering ARSI's specific expression in mature cartilage, it will be interesting to elucidate how the *Arsb*$^{-/-}$ phenotype compares with any skeletal defects in *Arsi*$^{-/-}$ models.

Our ARSI data highlight that the relationship between PG sulfatases and lysosomes is both biochemical and cell biological. Many PG sulfatases, such as ARSB, GALNS, and IDS, reside within lysosomes, where they participate in the stepwise degradation of glycosaminoglycans [8]. Our colocalization studies, using immunofluorescence and lysosomal markers, strongly suggest that ARSI also localizes to lysosomes, where it may function. Despite a report that ARSI did not colocalize with the lysosomal marker cathepsin D in the retinal-derived cell line ARPE-19 [38], EGFP-tagged ARSI colocalized with both LAMP1-positive lysosomes and RAB5-positive endosomes in HeLa cells, suggesting that it plays a role in the autophagy lysosomal pathway. From a biochemical perspective, lysosomal PG sulfatases show optimal activity in the acidic environment of lysosomes [40]. Further supporting its identity as a lysosomal PG sulfatase, ARSI showed C4S activity at pH of 4.5, but not at pH of 6.5, in our isolated cell-free system. This stands in contrast to a report showing extracellular ARSI activity at neutral conditions in ARPE-19 cells [38], but activity in that study was measured on an artificial substrate, and endogenous arylsulfatases of ARPE-19 show maximal activity at pH5–6. Future work could test whether ARSI can act as an endo-type sulfatase in neutral conditions. In humans, mutations to some PG sulfatases can cause various forms of mucopolysaccharidosis (MPS), a group of inherited lysosomal storage disorders (LSD's) characterized by the accumulation of partially-degraded GAGs within lysosomes [40]. Altered lysosome homeostasis is a diagnostic feature of LSD's, including MPS's [45], presumably as a compensatory mechanism for decreased lysosome-mediated catabolism. In this context, our findings of increased lysosome numbers and sizes in *Arsi*$^{-/-}$ chondrocytes underscore the importance of establishing and evaluating *Arsi*$^{-/-}$ animals as potential models of LSD's. In particular, *ARSI* mutations might underlie a new MPS in humans.

Our chemically-specific XRF imaging approach revealed that PG sulfation decreases during cartilage maturation. Previous studies using biochemical and histological methods suggested a reduction of C4S and C6S in mature cartilage of growth plates in fetal calves and juvenile chicks [5,7]. We confirmed that the sulfur signal in cartilage is comprised mostly of *O*-linked sulfate esters, which is the form of sulfur in sulfated PGs [29]. Indeed, we previously showed that cartilage of PG-deficient *fam20b* mutant zebrafish had reduced *O*-linked sulfate esters by XRF imaging [6]. We also illustrated for the first time the exact spatial distribution of PG sulfation across an intact growth plate. Interestingly, decreased PG sulfation in mature cartilage of the growth plate does not match previous studies showing higher sulfur levels in mature cartilage of articular cartilage in horses and pigs using X-ray emission techniques [46,47], suggesting differences in PG homeostasis of the transient growth plate and permanent articular cartilage.

Decreasing PG sulfation and ARSI expression during cartilage maturation have implications for understanding molecular mechanisms of endochondral ossification. As mentioned, PG desulfation occurs during PG degradation, so the decrease in PG sulfation might simply reflect ECM degradation during cartilage maturation, similar to collagen degradation by matrix metalloproteinase 13 [3]. Our FTIR data did not demonstrate significant PG degradation, however, and suggest another mechanism. Chondrocyte hypertrophy and perichondral bone formation were altered in animal models with reduced PG sulfation, such as brachymorphic (*bm*) and cartilage-matrix-deficient (*cmd*) mice; nanomelic (*nm*) chick; and f*am20b* and *xylt1* mutant zebrafish [22,48–50]. Sulfated PGs are known to bind growth factors and influence growth factor signalling, and aberrant signalling in many growth factor pathways has been described in developing cartilage of PG-defective animal models [22,51,52]. Therefore, decreased PG sulfation during normal cartilage maturation might release many growth factors, impacting several signalling pathways that can regulate multiple aspects of endochondral ossification. Indeed, a functional role for ARSI in endochondral ossification is supported by our *in vitro* findings of increased maturation markers in *Arsi*$^{-/-}$ chondrocytes. Taken together, our data suggest that ARSI might cause a decrease in PG sulfation during cartilage maturation, potentially altering growth factor-dependent aspects of endochondral ossification. Therefore, the establishment and analyses of *Arsi*$^{-/-}$ animal models is an important future direction of research, and *ARSI* mutations should be considered for human skeletal diseases of unknown etiology.

Materials and methods

Animal tissues

All animal experiments were approved by the University of Saskatchewan's Animal Research Ethics Board and adhered to the Canadian Council on Animal Care guidelines for humane use. White leghorn chicken eggs (University of Saskatchewan) were incubated in a humidified, rocking incubator at 37 °C, and C57/BL6 mouse embryos were collected from pregnant dams (University of Saskatchewan). Tissues were processed as previously described for histological and gene expression studies [33], unless otherwise detailed below, or for XRF imaging [6]. For FTIR analysis, sections were melted onto an IR-grade CaF_2 window (Crystran).

Histology

Chick limbs were subjected to acid-free Alizarin red and Alcian blue whole-mount staining, as previously described [49]. Chick humerus sections were stained with Safranin O, as described [53], but the Safranin O staining step was only 20 min for sample in Fig. 1C.

Section immunofluorescence

For unfixed sections adjacent to those imaged at the synchrotron, slides were dried at 60 °C for 30 min, fixed in 4 % PFA overnight at 4 °C, and rinsed twice in PBST (PBS/0.5 % triton- 100; Fisher Scientific). Alternatively, fixed sections were dried for 10 min, post-fixed in 4 % PFA at room temperature (RT) for 20 min, and rinsed twice in PBST. Afterwards, section immunos were performed as described [54]. Antibodies were: anti-COLX (X-AC9, Developmental Studies Hybridoma Bank (DSHB); 1:100); anti-COL2 (II-II6B3, DSHB; 1:100); anti-ARSI (SAB4501497, Sigma; 1:300); anti-GALNS (ab231647, Abcam; 1:100); anti-ARSB (ab85727, Abcam; 1:300); Alexa Fluor Plus 488 goat anti-rabbit IgG (H + L) (A32731, Thermo Fisher); Alexa Fluor Plus 488 goat anti-mouse IgG (H + L) (A32723, Thermo Fisher); Alexa Fluor 594 goat anti-rabbit IgG (H + L) (A11037, Thermo Fisher).

Synchrotron imaging and analyses

As previously described [6], XRF imaging of total sulfur was

performed at the VESPERS beamline, and chemically-specific XRF imaging and XANES measures were performed at the SXRMB beamline of the Canadian Light Source (Saskatoon, SK). Data processing was as described [6] with the following modifications. Immature and mature cartilage ROIs were drawn on the XRF image by importing the COLX immunofluorescence image from the adjacent tissue section in Adobe Photoshop CS6 (Adobe Inc., San Jose, CA) as a new layer, and total pixels and average pixel intensity were counted from the histogram.

Transcriptomic dataset

The mouse E14.5 RNAseq data are in the Gene Expression Omnibus (GEO) database (NIH) under accession GSE110051, and methods and statistics for data presented here were as published [33].

Human ARSI expression constructs

Each constructed plasmid was confirmed by sequencing the entire coding region and ligation joints. For overexpression experiments, a full-length form of ARSI was amplified from human placental cDNA library using a pair of primers for the first round of nested PCR; 5′ primer (5′-gccggcagatct**atg**cacaccctcactg-3′) containing *Bgl*II site (underlined) and the start codon (bold), and 3′ primer (5′-cagttttctcccagatctccatc-3′) containing *Bgl*II site (underlined). For second round of amplification, a pair of primers were used; 5′ primer (5′-gccggcagatct**atg**cacaccctcactg-3′) containing *Bgl*II site (underlined) and the start codon (bold), and 3′ primer (5′-tctcctctagaccatcagatccgttg-3′) containing *Bgl*II site (underlined). After adding an A-tail to the PCR fragment by Go Taq Flexi polymerase (Promega, Madison, WI), the cloned sequence was subcloned to pGEM-T easy vector (Promega) (pGEM-T ARSI(FL)). For ARSI-EGFP fusion, a 5′-primer (5′-tctcgagctcaagctaccatgcacaccctcact-3′), and a 3′-primer (5′-ggcgaccggtggatcgatccgttgggacattagc-3′) amplified ARSI from pGEM-T ARSI(FL), and this was cloned into pEGFP-N1 vector (Clontech, San Jose, CA), digested with *Hind*III and *BamH*I, based on site-specific recombination using the In-Fusion cloning kit (Clontech), creating pEGFP-N1-ARSI. Additionally, full-length human *ARSI* was cloned into pSP72-EF1-IRES-Blast vector.

For biochemical experiments, a truncated form of ARSI, lacking the first NH_2-terminal consisting of 24 amino acids, was amplified from human placental cDNA using a 5′ primer (5′-ccgagatctgtggccgacgggccc-3′) containing an in-frame *Bgl*II site (underlined) and a 3′ primer (5′-tctcccagatctccacca**tca**gatccgttg-3′) containing an in-frame *Bgl*II site (underlined) and the stop codon (bold). The PCR fragment was digested with *Bgl*II and subcloned into the *BamH*I site of the pEF-BOS/IP vector [55,56], resulting in pEF-BOS/IP-ARSI, where ARSI was fused to the insulin signal and protein A sequences.

HeLa lines and analyses

For immunolocalization and biochemical studies, pEGFP-N1-ARSI (2μg) and pEF-BOS/IP-ARSI) (2μg), respectively, were transfected into HeLa cells using Lipofectamine 3000 (Thermo Fisher Scientific, Waltham, MA) according to the manufacturer's instructions. For GAG and RT-qPCR analyses, pSP72-EF1-hARSI-IRES-Blast plasmid was linearized with ClaI and then transfected to HeLa cells using FuGENE6 (Promega). Transfected cells were selected with blasticidin and multiple clones stably expressing ARSI were established. To obtain negative control cells, pSP72-EF1-IRES-Blast empty vector was transfected to HeLa cells.

For **immunofluorescence**, HeLa cells cultured on a 3.5-cm glass-bottomed dish (AGC Techno Glass Co. Ltd., Shizuoka, Japan) were fixed with phosphate buffered saline (PBS) containing 4 % paraformaldehyde for 30 min on ice. After washing with PBS, cells were permeabilized with PBS containing 0.2 % Triton X-100 for 10 min at RT. After blocking with PBS containing 2 % bovine serum albumin (BSA) for 1 h at RT, cells were incubated overnight at 4 °C with the following antibodies: anti-GFP (M048–3; Medical & Biological Laboratories Co., Tokyo, Japan; 1:10,000), anti-LAMP1 (sc-17,768, Santa Cruz Biotechnology, Dallas, TX; 1:100) or anti-Rab5 (sc-10,767, Santa Cruz Biotechnology; 1:50). After washing with PBS, Alexa Fluor 488 secondary (Thermo Fisher Scientific; 1:400) or Alexa Fluor 594 secondary (Thermo Fisher Scientific; 1:400) was used for the detection of GFP or for LAMP1 and Rab5, respectively. Hoechst33342 was used as the nuclear counterstain. Images were acquired using a Zeiss LSM 700 confocal laser-scanning system (Carl Zeiss Inc., Oberkochen, Germany) equipped with an inverted Axio Observer Z1 microscope. For **RT-qPCR**, total RNA was extracted using High Pure RNA Isolation Kit (Roche) and reverse transcribed with MMLV reverse transcriptase. Real-time PCR was performed using FastStart Essential DNA Green Master (Roche) and LightCycler 96 System (Roche, Basel, Switzerland). Primers used for real-time PCR were as follows: (*ARSI*) F: 5′-caaggggtcaagttggaga-3′, R: 5′-cagcttctgtggcagtgtca-3′; (*B3GAT3*) F: 5′-cctgcctactatctatgttgttac, R: 5′-accaccaggtgtgtgaa-3′; (*CHST3*) F: 5′-tctgccattggcttgaac-3′, R: 5′-catgcagacatgaaatagcaaac-3′; (*CHST11*) F: 5′-aaacgccagcggaagaa-3′, R: 5′-gggatggcagagtgagtaga-3′; (*CHST12*) F: 5′-gagggaaagttctttgtttaagtg-3′, R: 5′-cggccttaacagccataat-3′; (*GAPDH*) F: 5′-atgggtgtgaaccatgagaagta-3′, R: 5′-ggcagtgatggcatggac-3′. For **GAG analysis**, cells were washed with PBS, collected using a cell scraper and homogenized in cold acetone. The dried powder was digested with actinase E (Kaken Pharmaceutical Co. Ltd., Tokyo, Japan) for 2 days at 55 °C. Trichloroacetic acid was added to the digested samples (final 5 %), and the soluble fraction was obtained. After extraction with diethyl ether, the aqueous phase was subjected to ethanol precipitation. The precipitate was dissolved in a pyridine-acetate buffer and gel-filtrated on a PD-MiniTrap G-25 column (Cytiva, Marlborough, MA). The flow-through fraction was collected, dried up, and dissolved in MilliQ water. An aliquot of the samples was digested with chondroitinase (ChABC from *Proteus vulgaris* and ChAC-II from *Arthrobacter aurescens* (both generously provided by Seikagaku Corp., Tokyo, Japan)). Digestions proceeded for 2 h at 37 °C and samples were derivatized with 2-aminobenzamide for 2 h at 65 °C. The derivatized samples were analyzed by high-performance liquid chromatography (CBM-20A, Shimadzu) on a YMC-Pack PA-G column (YMC Co., Ltd., Kyoto, Japan). Identification and quantification of the disaccharides were achieved by comparison with chondroitin sulfate disaccharide standard as described previously [57].

Cell-free polymeric CS biochemical analyses

COS-7 cells cultured in 10-cm dishes were transfected with 5 μg of pEF-BOS/IP-ARSI. Two days post-transfection, 1.4 ml of the culture medium was collected and incubated with 60 μl of IgG-Sepharose (Cytiva) for 2 h at 4 °C. Simultaneously, cells were lysed on ice for 30 min in 1 % Triton X-100 buffer (20 mM Tris–HCl, pH 7.5, 0.15 M NaCl, 1 mM EDTA-Na, and 10 % glycerol) containing a protease inhibitor cocktail (Nacalai Tesque, Kyoto, Japan) and 10 μM Z-Leu-Leu-Leu-H (aldehyde) (Peptide Institute Inc., Osaka, Japan). The lysate was then centrifuged at 13,500 rpm for 15 min at 4 °C, and the resulting supernatant was incubated with 60 μl of IgG-Sepharose for 2 h at 4 °C. The beads recovered by centrifugation were washed with 1 % NP40 buffer (20 mM Tris–HCl, pH 7.5, 0.15 M NaCl, 1 mM EDTA-Na, and 10 % glycerol) followed by Tris-buffered saline containing 0.1 % Tween (TBST). The expression of recombinant Protein A-fused ARSI was quantified by Western blotting using a Protein A standard (160–26,191, Fujifilm WAKO Chemicals, Osaka, Japan) at a known concentration.

Desulfation reactions were performed using chondroitin sulfate A (C4S) from whale cartilage or chondroitin sulfate C (C6S) from shark cartilage (both generously provided by Seikagaku Corporation, Tokyo, Japan) as acceptors. The molar ratios of various disaccharide units in these substrates—including C4S (ΔDi-4S), C6S (ΔDi-6S), and other minor units—were verified previously using HPLC analysis following chondroitinase digestion [58]. The reaction mixture (total volume 50 μl) consisted of 10 μg of C4S or C6S, 25 mM sodium acetate (pH 4.5) or 25 mM MES-NaOH (pH 6.5), 2 mM $CaCl_2$, 2 mM $MgCl_2$, and the

resuspended beads. After incubation at 37 °C for 5 h, the reaction was terminated by heating the mixture at 94 °C for 5 min. The mixture was centrifuged, and 5 µl of the supernatant was incubated with 5 munits of ChABC and ChAC-II at 37 °C for 4 h to ensure complete digestion into unsaturated disaccharides. The generated unsaturated disaccharides were subjected to fluorescent labeling and HPLC analysis, as described above.

RCS lines and analyses

RCS cells, a Swarm chondrosarcoma chondrocyte line [59], were cultured in DMEM High Glucose, supplemented with 10 % Fetal Bovine Serum, and 1 % penicillin/streptomycin (Euroclone). ARSI loss-of-function RCS clones were obtained through clustered regularly interspaced short palindromic repeats (CRISPR)/CRISPR-associated protein 9 (Cas9) technology. Briefly, 1×10^6 RCS chondrocytes were transfected with 5 µg of all-in-one vector (Sigma-Aldrich) containing the sgRNA of interest (B7 clone:_tcgtggtacccttggtcat; A2 clone:_gccatggtatcccacgtcg). 48 h after transfection, the cells were sorted for eGFP fluorescence using the BD FACSAria (BD Biosciences), grown to confluence, and then selected clones were subjected to PCR analysis followed by Sanger sequencing to identify mutations. For FGF18 treatment, cells were grown in 10 % FBS (Gibco). Day1 was one day after cells reached confluency, after which cells were treated with 50 ng/ml of human FGF18 (PeproTech) in 0.1 % BSA for 24 h for Day2 samples.

For **Western blot,** RCS chondrocytes were washed three times with PBS and collected using 1 % trypsin. The cell pellets were washed at least three times with PBS. Cells were lysed in RIPA lysis buffer (20 mM Tris [pH8.0], 150 mM NaCl, 0.1 % SDS, 1 % NP-40, 0.5 % sodium deoxycholate) supplemented with PhosSTOP and EDTA-free protease inhibitor tablets (Roche, Indianapolis, IN, USA), using freeze and thawing method. The soluble fractions were isolated by centrifugation at 18,000 g for 20 min at 4 °C. Total protein concentration in cellular extracts was measured using the colorimetric BCA protein assay kit (Pierce Chemical Co, Boston, MA, USA). Protein extracts, separated by SDS–PAGE and transferred onto PVDF, were probed with primary antibodies overnight against ARSI (HPA038398, Sigma-Aldrich; 1:300) and Filamin A (4762, Cell Signaling Technology; 1:1000). Proteins of interest were detected with HRP-conjugated goat anti-rabbit IgG antibody (Vector Laboratories; 1:2000) and visualized with the ECL Star Enhanced Chemiluminescent Substrate (Euroclone), according to manufacturer's protocol. Images were acquired using the ChemiDoc-lt imaging system (UVP). For **Lysotracker experiments**, LysoTracker DND99 (L7528 Thermo Fisher) was incubated at 50 nM in dark for 40 min at 37 °C. Cells were washed three times with PBS 1× and collected. Red fluorescence was measured by FACS Accuri C6, and 10,000 events were collected. For **immunofluorescence**, RCS chondrocytes were fixed for 10 min in 4 % PFA and permeabilized for 1 h in blocking buffer (0.05 % (w/v) saponin, 0.5 % (w/v) BSA, 50 mM NH4Cl, and 0.02 % NaN3 in PBS). Cells were incubated in humid chamber for 2 h at RT with anti-Lamp1 (ab24170, Abcam; 1:200), washed three times in PBS, incubated for 1 h with AlexaFluor secondary (1:400), washed again three times in PBS, incubated for 20 min with 1µg/ml Hoechst 33,342, and mounted in Mowiol (Sigma). Images were acquired using the LSM 880 confocal microscope equipped with a 63 × 1.4 numerical aperture oil objective, and image quantifications were performed using ImageJ plugins. For **transmission electron microscopy**, cells were fixed with 1 % glutaraldehyde in 0.2 M HEPES buffer (pH 7.4) for 30 min at RT and post-fixed as described [60]. After dehydration, the specimens were embedded in epoxy resin and polymerized at 60 °C for 72 h. Thin 60-nm sections were cut on a Leica EM UC7 microtome. EM images were acquired using a FEI Tecnai-12 electron microscope equipped with a VELETTA CCD digital camera (FEI, Eindhoven, The Netherlands). Morphometric analysis on the size of lysosomes was performed using iTEM software (Olympus SYS, Germany). For **GAG analyses**, medium from cultured cells was centrifuged at 5000 rpm 4 °C for 10 min, treated with Chondroitinase ABC (Sigma-Aldrich, cat# C3667) to release single CS non-sulfated and variously sulfated CS disaccharides, derivatized with a specific fluorochrome, and separated by HPLC-MS as previously published [61]. At the beginning of the study, Chondroitinase B (Sigma-Aldrich, cat# C8058), specific for dermatan sulfate (chondroitin sulfate B) was also tested, but no disaccharide product was observed, confirming the relatively low levels of dermatan sulfate. Consequently, chondroitinase ABC was used in all further analyses. For **RT-qPCR**, total RNA was extracted (Qiagen) from cells, and cDNA was synthesized with RevertAid cDNA synthesis kit (Thermo Fisher). RT-qPCR was performed with SsoAdvanced universal SYBR green supermix (Bio-Rad) using CFX96 rtPCR thermocycler device (Bio-Rad). Primer pairs were (*Cyc*, or *Ppia-ps1*, used as internal control) F: 5′-tggaaaagttgtaccccgga-3′, R: 5′-tacctccagtgccgtctcta-3′; (*Col2a1*) F: 5′-ccgatcccctgcagtacatg-3′, R: 5′-tgctctcgatctggttgttc-3′; (*Col10a1*) F: 5′-agctcacggaaaatgaccag-3′, R: 5′-gttctaagcgggggattagg-3′; (*Vegfa*) F: 5′- gtggaagaagaggcctggta-3′, R: 5′- cacacacacagccaagtctc-3′, as published [62]. *Mmp13* primers were designed as F: 5′-accagagaagtgtgacccag-3′, R: 5′- catggttgggaagttctggc-3′; To determine the relative expression of mRNA, 2-ΔΔCT method was used.

Statistical analysis

Statistically significant differences were determined by the one sample *t*-test, two-way ANOVA, unpaired *t*-test, or paired *t*-test, depending on the results being analyzed. The results are reported as mean ± standard error of the means. $p < 0.05$ was considered statistically significant.

Acknowledgements

Funding for this paper came from CIHR project grant 148683 (BFE). This work was supported in part by MEXT KAKENHI Scientific Research (B) 20H03386 and 24K02183 (to H. K.) and (C) 21K06089 (to S. N.), a Grant-in-Aid for Challenging Exploratory Research 22K19392 (to H.K.). We thank Rich Schneider for the chick *COL2A1* and *SPP1* RNA *in situ* probes and Ralph Marcucio for the chick *COL10A1* and *IHH* probes. Research described in this paper was performed at the VESPERS and SXRMB beamlines at the Canadian Light Source, which is supported by the Canada Foundation for Innovation, Natural Sciences and Engineering Research Council of Canada, the University of Saskatchewan, the Government of Saskatchewan, Western Economic Diversification Canada, the National Research Council Canada, and the Canadian Institutes of Health Research. We also acknowledge that, unfortunately and improperly, HeLa cells were developed several decades ago and distributed since without consent from the donor, Henrietta Lacks.

Supplementary materials

Supplementary material associated with this article can be found, in the online version, at doi:10.1016/j.matbio.2026.03.005.

Data availability

Data will be made available on request.

References

[1] G.L. Galea, M.R. Zein, S. Allen, P. Francis-West, Making and shaping endochondral and intramembranous bones. Developmental dynamics : an official publication of the, American Association of Anatomists 250 (2021) 414–449.
[2] B.F. Eames, L. de la Fuente, J.A. Helms, Molecular ontogeny of the skeleton, Birth Defects Research (Part C) 69 (2003) 93–101.
[3] N. Ortega, D. Behonick, D. Stickens, Z. Werb, How proteases regulate bone morphogenesis, Ann. N. Y. Acad. Sci. 995 (2003) 109–116.
[4] A.J. Deutsch, R.J. Midura, A.H. Plaas, Structure of chondroitin sulfate on aggrecan isolated from bovine tibial and costochondral growth plates, J. Orthop. Res. 13 (1995) 230–239.

[5] C. Farquharson, C.C. Whitehead, N. Loveridge, Alterations in glycosaminoglycan concentration and sulfation during chondrocyte maturation, Calcif. Tissue Int. 54 (1994) 296–303.
[6] M.J. Hackett, G.N. George, I.J. Pickering, B.F. Eames, Chemical biology in the embryo, in: *Situ* Imaging of Sulfur Biochemistry in Normal and Proteoglycan-Deficient Cartilage Matrix. Biochemistry, 55, 2016, pp. 2441–2451.
[7] R.E. Wuthier, A zonal analysis of inorganic and organic constituents of the epiphysis during endochondral calcification, Calcif. Tissue Res. 4 (1969) 20–38.
[8] D.S. Brown, B.F. Eames, Emerging tools to study proteoglycan function during skeletal development, Methods Cell Biol. 134 (2016) 485–530.
[9] C.B. Knudson, W. Knudson, Cartilage proteoglycans, Semin. Cell Dev. Biol. 12 (2001) 69–78.
[10] Gray, H., Williams, P.L., 1989. Gray's anatomy. C. Livingstone, Edinburgh; New York.
[11] M. Kusche-Gullberg, L. Kjellén, Sulfotransferases in glycosaminoglycan biosynthesis, Curr. Opin. Struct. Biol. 13 (2003) 605–611.
[12] M. Sardiello, I. Annunziata, G. Roma, A. Ballabio, Sulfatases and sulfatase modifying factors: an exclusive and promiscuous relationship, Hum. Mol. Genet. 14 (2005) 3203–3217.
[13] R.S. Holmes, Comparative and evolutionary studies of mammalian arylsulfatase and sterylsulfatase genes and proteins encoded on the X-chromosome, Comput. Biol. Chem. 68 (2017) 71–77.
[14] M. Stam, P. Lelievre, M. Hoebeke, E. Corre, T. Barbeyron, G. Michel, SulfAtlas, the sulfatase database: state of the art and new developments, Nucleic. Acids. Res. 51 (2023) D647–D653.
[15] L. Schlotawa, L.A. Adang, K. Radhakrishnan, R.C. Ahrens-Nicklas, Multiple sulfatase deficiency: a disease comprising mucopolysaccharidosis, sphingolipidosis, and more caused by a defect in posttranslational modification, Int. J. Mol. Sci. 21 (2020).
[16] C. Settembre, R.M. Perera, Lysosomes as coordinators of cellular catabolism, metabolic signalling and organ physiology, Nat. Rev. Mol. Cell Biol. 25 (2024) 223–245.
[17] H.G. Hers, Inborn lysosomal diseases, Gastroenterology 48 (1965) 625–633.
[18] K. Dzobo, T. Turnley, A. Wishart, A. Rowe, K. Kallmeyer, F. van Vollenstee, N. Thomford, C. Dandara, D. Chopera, M. Pepper, M. Parker, Fibroblast-derived extracellular matrix induces chondrogenic differentiation in Human adipose-derived mesenchymal stromal/stem cells *in vitro*, Int. J. Mol. Sci. 17 (2016), 1259-1259.
[19] C.I. Gama, S.E. Tully, N. Sotogaku, P.M. Clark, M. Rawat, N. Vaidehi, W. A. Goddard, A. Nishi, L.C. Hsieh-Wilson, Sulfation patterns of glycosaminoglycans encode molecular recognition and activity, Nat. Chem. Biol. 2 (2006) 467–473.
[20] Y. Gao, S. Liu, J. Huang, W. Guo, J. Chen, L. Zhang, B. Zhao, J. Peng, A. Wang, Y. Wang, W. Xu, S. Lu, M. Yuan, Q. Guo, The ECM-cell interaction of cartilage extracellular matrix on chondrocytes, BioMed. Res. Int. 2014 (2014).
[21] N.O. Chahine, F.H. Chen, C.T. Hung, G.A. Ateshian, Direct measurement of osmotic pressure of glycosaminoglycan solutions by membrane osmometry at room temperature, Biophys. J. 89 (2005) 1543–1550.
[22] M. Cortes, A.T. Baria, N.B. Schwartz, Sulfation of chondroitin sulfate proteoglycans is necessary for proper Indian hedgehog signaling in the developing growth plate, Development 136 (2009) 1697–1706.
[23] B. Gualeni, M. Facchini, F. De Leonardis, R. Tenni, G. Cetta, M. Viola, A. Passi, A. Superti-Furga, A. Forlino, A. Rossi, Defective proteoglycan sulfation of the growth plate zones causes reduced chondrocyte proliferation via an altered Indian hedgehog signalling, Matrix Biol. 29 (2010) 453–460.
[24] C. Settembre, I. Annunziata, C. Spampanato, D. Zarcone, G. Cobellis, E. Nusco, E. Zito, C. Tacchetti, M.P. Cosma, A. Ballabio, Systemic inflammation and neurodegeneration in a mouse model of multiple sulfatase deficiency, Proc. Natl. Acad. Sci. U.S.A. 104 (2007) 4506–4511.
[25] C. Settembre, E. Arteaga-Solis, M.D. McKee, R. de Pablo, Q. Al Awqati, A. Ballabio, G. Karsenty, Proteoglycan desulfation determines the efficiency of chondrocyte autophagy and the extent of FGF signaling during endochondral ossification, Genes Dev. 22 (2008) 2645–2650.
[26] J. Muenzer, Overview of the mucopolysaccharidoses, Rheumatology (Oxford, England) 50 (Suppl 5) (2011) v4–12.
[27] A.M. Montano, S. Tomatsu, G.S. Gottesman, M. Smith, T. Orii, International Morquio A Registry: clinical manifestation and natural course of Morquio A disease, J. Inherit. Metab. Dis. 30 (2007) 165–174.
[28] V. Valayannopoulos, H. Nicely, P. Harmatz, S. Turbeville, Mucopolysaccharidosis VI, Orphanet. J. Rare Dis. 5 (2010) 5.
[29] T. Mikami, H. Kitagawa, Biosynthesis and function of chondroitin sulfate, Biochim. Biophys. Acta 1830 (2013) 4719–4733.
[30] A. Boskey, N. Pleshko Camacho, FT-IR imaging of native and tissue-engineered bone and cartilage, Biomaterials 28 (2007) 2465–2478.
[31] S. Saarakkala, P. Julkunen, Specificity of fourier transform infrared (FTIR) microspectroscopy to estimate depth-wise proteoglycan content in normal and osteoarthritic human articular cartilage, Cartilage 1 (2010) 262–269.
[32] L. Rieppo, J. Rieppo, J.S. Jurvelin, S. Saarakkala, Fourier transform infrared spectroscopic imaging and multivariate regression for prediction of proteoglycan content of articular cartilage, PLoS One 7 (2012) e32344-e32344.
[33] P. Gomez-Picos, K. Ovens, A.M. Ashique, M. Hassanzadeh, I. McQuillan, B. F. Eames, Chondrocyte maturation bridges two cross-inhibitory subnetworks of the skeletal cell gene regulatory network, Development 152 (2025).
[34] A. Amores, A. Force, Y.L. Yan, L. Joly, C. Amemiya, A. Fritz, R.K. Ho, J. Langeland, V. Prince, Y.L. Wang, M. Westerfield, M. Ekker, J.H. Postlethwait, Zebrafish hox clusters and vertebrate genome evolution, Science 282 (1998) 1711–1714.
[35] J.J. Moss, C.L. Hammond, J.D. Lane, Zebrafish as a model to study autophagy and its role in skeletal development and disease, Histochem. Cell Biol. 154 (2020) 549–564.
[36] A. Kurimchak, D.S. Haines, J. Garriga, S. Wu, F. De Luca, M.J. Sweredoski, R. J. Deshaies, S. Hess, X. Grana, Activation of p107 by fibroblast growth factor, which is essential for chondrocyte cell cycle exit, is mediated by the protein phosphatase 2A/B55alpha holoenzyme, Mol. Cell Biol. 33 (2013) 3330–3342.
[37] B.F. Eames, J.A. Helms, Conserved molecular program regulating cranial and appendicular skeletogenesis. Developmental dynamics : an official publication of the, American Association of Anatomists 231 (2004) 4–13.
[38] M. Oshikawa, R. Usami, S. Kato, Characterization of the arylsulfatase I (ARSI) gene preferentially expressed in the human retinal pigment epithelium cell line ARPE-19, Mol. Vis. 15 (2009) 482–494.
[39] A.J. Obaya, Molecular cloning and initial characterization of three novel human sulfatases, Gene 372 (2006) 110–117.
[40] G. Diez-Roux, A. Ballabio, Sulfatases and HUMAN disease, Annu Rev. Genomics. Hum. Genet. 6 (2005) 355–379.
[41] I. Kalus, B. Salmen, C. Viebahn, K. von Figura, D. Schmitz, R. D'Hooge, T. Dierks, Differential involvement of the extracellular 6-O-endosulfatases Sulf1 and Sulf2 in brain development and neuronal and behavioural plasticity, J. Cell Mol. Med. 13 (2009) 4505–4521.
[42] A. Ratzka, S. Mundlos, A. Vortkamp, Expression patterns of sulfatase genes in the developing mouse embryo, Dev. Dyn. 239 (2010) 1779–1788.
[43] G. Hendrickx, T. Danyukova, A. Baranowsky, T. Rolvien, A. Angermann, M. Schweizer, J. Keller, J. Schroder, C. Meyer-Schwesinger, N. Muschol, C. Paganini, A. Rossi, M. Amling, S. Pohl, T. Schinke, Enzyme replacement therapy in mice lacking arylsulfatase B targets bone-remodeling cells, but not chondrocytes, Hum. Mol. Genet. 29 (2020) 803–816.
[44] S. Pohl, A. Angermann, A. Jeschke, G. Hendrickx, T.A. Yorgan, G. Makrypidi-Fraune, A. Steigert, S.C. Kuehn, T. Rolvien, M. Schweizer, T. Koehne, M. Neven, O. Winter, R.V. Velho, J. Albers, T. Streichert, J.M. Pestka, C. Baldauf, S. Breyer, R. Stuecker, N. Muschol, T.M. Cox, P. Saftig, C. Paganini, A. Rossi, M. Amling, T. Braulke, T. Schinke, The lysosomal protein arylsulfatase B is a key enzyme involved in skeletal turnover, J. Bone Miner. Res. 33 (2018) 2186–2201.
[45] L. Bajaj, P. Lotfi, R. Pal, A.D. Ronza, J. Sharma, M. Sardiello, Lysosome biogenesis in health and disease, J. Neurochem. 148 (2019) 573–589.
[46] T. Reinert, U. Reibetanz, J. Vogt, T. Butz, A. Werner, W. Gründer, Spatially resolved elemental distributions in articular cartilage, Nucl. Instrum. Methods Phys. Res. Section B: Beam Interactions with Materials and Atoms 181 (2001) 516–521.
[47] R. Rizzo, M. Grandolfo, C. Godeas, K.W. Jones, F. Vittur, Calcium, sulfur, and zinc distribution in normal and arthritic articular equine cartilage: a synchrotron radiation-induced X-ray emission (SRIXE) study, J. Exp. Zool. 273 (1995) 82–86.
[48] M.S. Domowicz, M. Cortes, J.G. Henry, N.B. Schwartz, Aggrecan modulation of growth plate morphogenesis, Dev. Biol. 329 (2009) 242–257.
[49] B.F. Eames, Y.L. Yan, M.E. Swartz, D.S. Levic, E.W. Knapik, J.H. Postlethwait, C. B. Kimmel, Mutations in fam20b and xylt1 reveal that cartilage matrix controls timing of endochondral ossification by inhibiting chondrocyte maturation, PLoS Genet. 7 (2011) e1002246.
[50] H. Watanabe, K. Kimata, S. Line, D. Strong, L.-y. Gao, C.A. Kozak, Y. Yamada, Mouse cartilage matrix deficiency (cmd) caused by a 7 bp deletion in the aggrecan gene, Nat. Genet. 7 (1994) 154–157.
[51] M. Kluppel, T.N. Wight, C. Chan, A. Hinek, J.L. Wrana, Maintenance of chondroitin sulfation balance by chondroitin-4-sulfotransferase 1 is required for chondrocyte development and growth factor signaling during cartilage morphogenesis, Development 132 (2005) 3989–4003.
[52] E. Koosha, C.T.A. Brenna, A.M. Ashique, N. Jain, K. Ovens, T. Koike, H. Kitagawa, B.F. Eames, Proteoglycan inhibition of canonical BMP-dependent cartilage maturation delays endochondral ossification, Development 151 (2024).
[53] J.F.A. McManus, R.W. Mowry, Staining methods: Histologic and Histochemical, Paul B. Hoeber, 1960.
[54] B.F. Eames, R.A. Schneider, Quail-duck chimeras reveal spatiotemporal plasticity in molecular and histogenic programs of cranial feather development, Development 132 (2005) 1499–1509.
[55] S. Mizushima, S. Nagata, pEF-BOS, a powerful mammalian expression vector, Nucleic. Acids. Res. 18 (1990) 5322.
[56] S. Nadanaka, E. Purunomo, N. Takeda, J. Tamura, H. Kitagawa, Heparan sulfate containing unsubstituted glucosamine residues: biosynthesis and heparanase-inhibitory activity, J. Biol. Chem. 289 (2014) 15231–15243.
[57] H. Kitagawa, A. Kinoshita, K. Sugahara, Microanalysis of glycosaminoglycan-derived disaccharides labeled with the fluorophore 2-aminoacridone by capillary electrophoresis and high-performance liquid chromatography, Anal. Biochem. 232 (1995) 114–121.
[58] S. Nadanaka, M. Ishida, M. Ikegami, H. Kitagawa, Chondroitin 4-O-sulfotransferase-1 modulates wnt-3a signaling through control of E disaccharide expression of chondroitin sulfate, J. Biol. Chem. 283 (2008) 27333–27343.
[59] K.B. King, J.H. Kimura, The establishment and characterization of an immortal cell line with a stable chondrocytic phenotype, J. Cell. Biochem. 89 (2003) 992–1004.
[60] E.V. Polishchuk, A. Merolla, J. Lichtmannegger, A. Romano, A. Indrieri, E. Y. Ilyechova, M. Concilli, R. De Cegli, R. Crispino, M. Mariniello, R. Petruzzelli, G. Ranucci, R. Iorio, F. Pietrocola, C. Einer, S. Borchard, A. Zibert, H.H. Schmidt, E. Di Schiavi, L.V. Puchkova, B. Franco, G. Kroemer, H. Zischka, R.S. Polishchuk, Activation of autophagy, observed in liver tissues from patients with Wilson

disease and from ATP7B-deficient animals, protects hepatocytes from copper-induced apoptosis, Gastroenterology 156 (2019) 1173–1189, e1175.
[61] N. Volpi, F. Galeotti, B. Yang, R.J. Linhardt, Analysis of glycosaminoglycan-derived, precolumn, 2-aminoacridone-labeled disaccharides with LC-fluorescence and LC-MS detection, Nat. Protoc. 9 (2014) 541–558.
[62] L. Cinque, M. Iavazzo, G. Di Bonito, E. Polishchuk, R. De Cegli, C. Settembre, FGF signaling promotes lysosome biogenesis in chondrocytes via the Mannose phosphate receptor pathway, Traffic 26 (2025) e70013.